NASA Technical Memorandum 81913

Laser Velocimetry Technique Applied to the Langley 0.3-Meter Transonic Cryogenic Tunnel

Luther R. Gartrell, Paul B. Gooderum,
William W. Hunter, Jr., and James F. Meyers
Langley Research Center
Hampton, Virginia

National Aeronautics
and Space Administration

**Scientific and Technical
Information Branch**

1981

SUMMARY

A low-power (15 mW) laser velocimeter operating in the forward-scatter mode has been used to measure free-stream mean velocities in the Langley 0.3-Meter Transonic Cryogenic Tunnel. Velocity ranging from 51 to 235 m/s was measured with at least ±1-percent accuracy. These measurements were obtained for a variety of nominal tunnel conditions: Mach numbers from 0.20 to 0.77, total temperatures from 100 to 250 K, and pressures 101 to 152 kPa (1.0 to 1.5 atm). Particles were not injected to augment the existing Mie scattering material. It is postulated that the existing light scattering material in these tests was liquid nitrogen droplets normally injected to control the tunnel temperature. Signal levels obtained during the tests indicated that the average particulate diameter was greater than 1.0 m. Tunnel vibrations and thermal effects, which were considered to be potential problems before the tests, had no detrimental effects on the optical system.

INTRODUCTION

During the past several years, laser velocimeter (LV) techniques have been successfully applied to flow velocity measurements in aerodynamic test facilities (refs. 1 to 5). The nonintrusive, LV technique reduces the probability of flow disturbances, often experienced with probe-type techniques. In this technique, the velocity of particles present in the flow is equated to the gas velocity; thus the need is eliminated for calibrations or knowledge of other flow parameters such as temperature and pressure.

With the increasing interest in aircraft efficiency at high speed, the aerodynamic flow characteristics for full-scale Reynolds number simulation in the transonic regime are important. In a given wind tunnel with a specified gas, the Reynolds number can be increased by increasing the pressure and/or lowering the temperature. An accepted method for increasing the Reynolds number is by cryogenic cooling.

This paper describes the results of LV tests conducted in the Langley 0.3-Meter Transonic Cryogenic Tunnel. The purpose of the tests was to investigate the problems and potential use of this technique for measuring the flow velocity characteristics in this unique wind tunnel. A low-power one-component LV system operated in the forward-scatter mode was used to make a series of free-stream velocity measurements without a model in the test section. The naturally occurring Mie scattering particulates used in these tests are postulated to be residual droplets resulting from the injected liquid nitrogen (LN_2) which is used to maintain the desired temperature in the tunnel. The optics, electronics, data processing equipment and procedures, and general tunnel operating procedure and characteristics are described in this paper.

Also presented are results of the LV tests which recommend that the laser velocimeter be further investigated for future use in this facility.

SYMBOLS

d	half-amplitude vibration displacement, cm
$E\{\ \}$	expected value
F_x	longitudinal function
F_y	vertical function
f	vibration frequency, Hz
f_c	reference clock frequency, MHz
f_D	Doppler frequency, MHz
g	gravitational acceleration
M	number of threshold crossings
M_∞	free-stream Mach number
N	number of velocity measurements in ensemble
n	exponent in data from high-speed burst counter
q	$= f_D/Mf_c$
R_{xy}	cross correlation function
S_f	fringe spacing, μm
S_{xy}	cross spectral density
T	integration time
T_t	total temperature, K
V	absolute velocity component normal to fringes, m/s
V_c	calculated velocity, m/s
V_i	individual velocity measurement, m/s
V_m	measured velocity, m/s
x	longitudinal direction
γ	true turbulence intensity, $\sigma/\bar{V}$
γ_m	measured turbulence intensity

Δ	uncertainty
ε_V	error in mean velocity
ε_γ	error in turbulence intensity
η_i	random variable
θ	angle between intersecting laser beams, deg
λ	laser wavelength, nm
σ	true standard deviation, m/s
σ_m	measured standard deviation, m/s
τ	delay time

A bar over a symbol denotes arithmetic mean.

TECHNIQUE AND APPARATUS

Wind Tunnel

A schematic diagram of the Langley 0.3-Meter Transonic Cryogenic Tunnel is shown in figure 1. It is a continuous-flow, fan-driven pressure tunnel which uses nitrogen as a test gas. The very cold temperatures required for high Reynolds number testing are achieved by direct injection of liquid nitrogen (LN_2) just downstream of the test section. Stagnation temperatures from 77 to 339 K, stagnation pressures of 1.2 to 6.0 atm (1 atm = 101 kPa), and Mach numbers from 0.05 to 0.95 (the exact range depending upon the total temperature) can be attained by varying the rates of liquid nitrogen injection and gaseous nitrogen venting and the fan speed. The combined low temperature and high pressure can provide Reynolds numbers exceeding 330 million per meter. The tunnel is constructed of welded 6061-T6 aluminum alloy and encased in a fiberglass thermal blanket except for the test section access flange bolts and metal optics enclosures. The 12-bladed fan is driven by a 2.2-MW variable frequency motor.

This facility is equipped with a 0.20 × 0.61 m, two-dimensional test section for airfoil testing which has four quartz windows. Two of these windows are located in the tunnel sidewalls and are D-shaped to permit observation of the flow over the top of an airfoil. The other two are pressure windows located on the same optical axis between the plenum and the optics enclosures mounted on the test section. These pressure windows serve to contain the cryogen at whatever pressure the tunnel is being operated.

The liquid nitrogen supply system consists of two, 106-m^3 tanks which supply the liquid nitrogen to a pump. The pump supplies liquid nitrogen to the tunnel pressures up to 1.2 MPa (175 psig) at 0.0094 m^3/s to four digitally controlled LN_2 supply valves. The liquid nitrogen is injected through these valves

downstream of the tunnel test section through four flush-mounted fan spray nozzles in the diffuser. The liquid nitrogen jet is atomized as it enters the tunnel flow.

A venting subsystem allows removal of excess gas in order to maintain existing tunnel pressure as liquid nitrogen is injected to obtain the desired operating temperature. A more detailed description of tunnel design and operation is given in reference 6.

Laser Velocimeter Technique

The basic principle of laser velocimetry depends on Mie scattering and the Doppler effect. The fundamentals involved can be explained by considering the fringe model shown in figure 2. The laser beam is split into two parallel beams of approximately equal intensity. A lens focuses the beams to a common point. Being coherent (temporal and spatial), the interacting wave fronts of the beam form interference fringes within an ellipsoidal region (sample volume) which is approximately centered at the focal plane. (The size of the sample region depends on the beam separation, the beam diameter, and the lens focal length.) The fringe pattern is a combination of alternating light and dark regions of equal spacing. The spacing S_f is given by

$$S_f = \frac{\lambda}{2 \sin (\theta/2)}$$

where λ is the wavelength of the laser light and θ is the angle between the optical axes of the intersecting beams. If a particle in the moving fluid passes through the fringes, it scatters light from the two incident laser beams. This scattered light has a sinusoidal intensity variation with time. The frequency of intensity variation is a function of the fringe spacing and of the particle velocity in the direction normal to the fringes. The optical signal (Doppler shifted frequency) is converted by a photodetector into an electrical burst signal with frequency f_D given by

$$f_D = \frac{2V \sin (\theta/2)}{\lambda}$$

where V is the component of the absolute particle velocity perpendicular to the fringe pattern.

Optical System

The LV optics used in the tunnel tests discussed herein were configured to operate in the forward-scatter mode and to measure the axial component of

the flow velocity. A diagram of the system is shown in figure 3. It uses a He-Ne laser operating in the TEM_{00} mode and providing 15 mW of continuous power at a wavelength of 632.8 nm. The laser beam is divided into two parts by a 50:50 beam splitter prism which yields a beam separation of 50 mm. A transmitter lens with focal length of 47.62 cm was used to focus the beams to a spot size (sample volume) 0.20 mm in diameter by 3 mm long. The light scattered by particles in the sample volume is collected by an F1:2 lens and is imaged on a high-gain, low-noise photomultiplier tube (PMT) with an S-20 wavelength response by a 10× (0.25 numerical aperture) microscope objective lens. The LV optical system was mounted in metal enclosures designed to house a schlieren system. This was done so that the enclosures could be purged with dry room temperature nitrogen and wrapped with heater tape to prevent moisture from condensing on the viewing windows (fig. 4). The optics installed in these enclosures are shown in figure 5.

Signal Conditioning Electronics

The signal conditioning electronics incorporated a 10-dB-gain wideband amplifier, a high-speed burst counter, and a minicomputer plus peripheral equipment. The high-speed burst counter is a real-time (time domain) device which uses a direct counting approach for measuring the time it takes for a particle to traverse a preset number of successive fringes. This time is measured with a resolution of 2 ns. The counter is equipped with band-pass filters for removing the pedestal voltage and with a double-threshold zero-crossing detector and comparator circuit for noise rejection. Data that have been validated are placed in a storage register which has a 16-bit binary output interface with a minicomputer. The data output format (10 data bits, four exponent bits) permits measuring a Doppler frequency range from 1.2 kHz to 100 MHz. These data are fed into a minicomputer (binary form) which is programmed to calculate the Doppler frequency from the following conversion equation:

$$\text{Frequency} = \frac{3.2 \times 10^{10}}{2^{n} \times \text{Reading}}$$

where the values of the exponent n and the reading are provided by the high-speed burst counter. For more detailed discussion of the digital counter, see reference 3.

Data Acquisition and Processing

The digital output from the high-speed burst counter is input to a 16-bit data acquisition and processing minicomputer where it is stored on a 0.5-megabyte floppy disk for later final processing. On-line data processing consists of the calculation of the basic statistical characteristics of an ensemble of velocity measurements. These results along with a plot of the measured velocity ensemble

histogram are displayed on a cathode-ray tube (CRT) terminal. The block diagram of the system is shown in figure 6.

Data acquisition from the high-speed burst counter is controlled by the minicomputer through full handshake interaction. The maximum data acquisition rate of 20 000 measurements per second was sufficient to obtain the data in the present test since the average data rate was between 10 and 20 measurements per second. Each velocity ensemble consisted of 1024 measurements and the average data acquisition time was approximately 90 seconds.

Once the velocity ensemble has been acquired, the ensemble arithmetic mean and standard deviation are calculated. Data measured by the high-speed burst counter greater than three standard deviations from the mean are considered spurious and therefore are deleted from the ensemble. The calculated mean value is then subtracted from the remaining data in the ensemble to maximize precision in the remaining statistical calculations, since single precision (6 decimal places) floating point numbers are used in the minicomputer. A new arithmetic mean and standard deviation are calculated based on the adjusted ensemble with the mean removed. If there are no spurious data points, the new mean is equal to zero; if there are, the new mean represents the difference between the previously calculated mean and the true measurement mean. Thus the algebraic addition of the previous arithmetic mean and the new arithmetic mean yield the true measurement mean velocity of the velocity ensemble. Likewise the new standard deviation represents the true standard deviation of the velocity ensemble since the spurious data were deleted from the ensemble. In addition to the mean and standard deviation, the following statistical quantities are also calculated: statistical uncertainty in the mean, statistical uncertainty in the standard deviation, normalized standard deviation, and the skew and excess of the ensemble. These results along with the histogram of the ensemble (1.0 m/s resolution) were displayed on the CRT terminal and a hard copy of the CRT display was produced. An example of the CRT display is shown in figure 7.

ERROR ANALYSIS

The accuracy of velocity measurement using the laser velocimeter is dependent upon the accuracy with which the particle follows the fluid flow, gradients within the flow field, errors derived from the optical and electronic systems, and measurement uncertainties due to the statistics of the measured velocity ensemble. In the present test, the free-stream velocity was measured in an empty test section; there were no detectable effects on the measurements due to velocity gradients within the velocimeter sample volume. Further, the velocity lag experienced by the particles as the flow accelerates in the tunnel throat was not apparently significant since the standard deviations of the measurement ensembles were small and reasonably symmetric, even though the distribution of the liquid nitrogen particle sizes was suspected to be large ($>>1.0$ μm in diameter) based on the signal levels received from the laser velocimeter. Since the velocity gradients were negligible and the measured standard deviations were small, the following errors should also be negligible:

1. Particle tracking errors (inability of particles to follow the flow field and related velocity broadening due to the size distribution of the particles)

2. Velocity bias (the probability that a larger number of faster particles will be measured than slower particles per unit time)

3. Measurement dead zone (particles passing through the sample volume with a trajectory that crosses too few fringes to yield a measurement)

4. Velocity gradient errors (velocity gradient across the sample volume yielding a broadening of the velocity distribution which is not due to turbulence)

5. Sample volume position (unfaithful representation of the flow field due to position inaccuracy)

However, the remaining error sources must be considered:

1. Cross-beam angle measurement error and nonparallelism of the fringes

2. Threshold limit error, clock synchronization error, and quantizing error in the high-speed burst counter

3. Uncertainties in the statistical calculations of the measurement ensembles

The two error sources due to the optical system are cross-beam angle measurement and fringe nonparallelism. The cross-beam angle error is a velocity bias due to the uncertainty in locating the center of the laser beam during the geometric measurement of the angle. The uncertainty band is estimated to yield a bias uncertainty in velocity of ±0.6 percent for the present optical system. The fringes within the sample volume diverge if the spatial location of the waist of each laser beam is not located at the beam crossover point. In the present system, the waist for each beam extends 3 cm on both sides of the crossover point; thus, the errors due to fringe nonparallelism are reduced to an insignificant level.

The three error sources in the electronic systems, threshold limit error, clock synchronization error, and quantizing error, are developed in detail in the appendix. Although the threshold limit error does not apply for the high-speed burst counter used in the present test, the clock synchronization and quantizing errors do and are dependent upon the mean velocity. As an example of their magnitudes, a worst case condition is used: mean velocity of 235 m/s and an ensemble standard deviation of 1.68 m/s. Clock synchronization yields a bias error in the mean velocity of 0.47 percent and a bias error in the normalized standard deviation of 0.47 percent. Quantizing yields a random error in the mean velocity of 0.0003 percent and a bias error in the normalized standard deviation of 29.4 percent. In the present test, the normalized standard deviation measurements were corrected for quantizing error, but not for clock synchronization error. The mean velocity bias error due to clock synchronization was not removed.

Estimates of the system error sources in the velocity are summarized in the following table:

Velocity error source	Bias, percent	Random, percent
Cross-beam angle	±0.6	------
Diverging fringes	Negligible (<<0.01)	------
Clock synchronization	0.47	------
Quantizing	------	Negligible (<<0.001)

The final error source is the statistical uncertainty in estimating the true mean and standard deviation of the velocity of the flow. These errors depend on the number of particle velocity measurements included in the ensemble and the magnitude of the standard deviation of the ensemble. These uncertainties, presented in table I for each ensemble, average approximately 0.03 percent for the mean velocity and 3.5 percent for the standard deviation.

TEST PROCEDURE

The tunnel is cooled prior to operation by running the drive motor and fan at a low speed and injecting liquid nitrogen at a low flow rate. After reaching the desired operating temperature, the tunnel flow is brought to the desired Mach number and pressure by adjusting the drive fan speed, controlling the quantity of liquid nitrogen being injected, and regulating the amount of nitrogen gas vented to the atmosphere. For the tests discussed herein, the nominal free-stream temperatures range from 100 to 250 K and Mach numbers from 0.20 to 0.77. The laser velocimeter was adjusted to measure the axial free-stream velocity component along the test section centerline as shown in figure 8. The test section was empty. For these tests, naturally occurring particulates (postulated to be LN_2 droplets) provided the light scattering particles necessary for the LV operation. Vibration levels on both sides of the test section were measured with a triaxial accelerometer mounted on the optics enclosures approximately 0.5 m from the test section wall.

RESULTS AND DISCUSSION

While preparing the tunnel for this series of tests, edge cracks were found in one of the pressure windows. Safety considerations required that the tunnel be operated at the lowest practical differential pressure without exceeding 1.0 to 1.5 atm in the plenum. Therefore, the conditions were limited to a Mach number range from 0.20 to 0.77 and a stagnation pressure of 1.5 atm.

At the colder operating temperatures (100 K), the tunnel test section walls, with the viewing ports, could contract by approximately 0.32 cm. Refraction effects caused by this dimensional change had no detectable effect on the LV optical alignment. Thermostatically controlled heater tape wrapped around the optics enclosures kept the internal ambient temperature above 266 K. Dry nitrogen gas purged through the optics enclosures kept the viewing ports free of condensation.

Vibration Measurements

The induced vibrations most critical to the optical alignment are the longitudinal mode (parallel to the flow) and the vertical mode (normal to the flow), with the worst cases occurring at the higher Mach numbers and temperatures. Typical results of vibration measurements for the transmitter and receiver optics enclosures (figs. 9 and 10) show distinct peaks at 100 and 400 Hz. Since the displacement varies inversely with the square of the frequency, 100 Hz represents the larger displacement. At 100 Hz, the longitudinal and vertical vibration levels at the transmitter and receiver were on the order of 0.32g. The half-amplitude displacement, approximated by

$$d \approx \frac{24.84g}{f^2}$$

is 8×10^{-4} cm. Coupling between the vibration measurements for the transmitter and receiver enclosures was determined by computing the cross spectral density, which is expressed as

$$S_{xy}(\omega) = \int_{-\infty}^{\infty} R_{xy}(\tau)\, e^{-j\omega\tau}\, d\tau$$

where ω is the angular frequency, $j = \sqrt{-1}$, and $R_{xy}(\tau)$ is the cross correlation function given by

$$\lim_{T \to \infty} \left(\frac{1}{2T}\right) \int_{-T}^{T} F_x(t)\, F_y(t - \tau)\, dt$$

with T being the integration time and τ the delay. Typical cross spectral density plots are shown in figure 11. For the range of test conditions, the vibration levels were not severe enough to affect the optical alignment or the laser operation.

Velocity Measurements

Free-stream axial mean velocity measurements as a function of Mach number and temperature are shown in figure 12. A comparison of the measured velocities ($\bar{V}_m$) and those calculated from tunnel parameters ($\bar{V}_c$) (shown in fig. 13) indicates good agreement, typically better than 1 percent. The standard deviations for this plot cannot be shown because they would appear within the test-point symbols. A plot of the normalized standard deviation ($\sigma_m/\bar{V}_m$) is shown in figure 14. Over the test Mach number and temperature range, the normalized standard deviation was usually less than 1 percent. The velocity measurement data and nominal tunnel conditions are listed in table I. The size of the particles (LN_2 droplets) from which these measurements were obtained was not determined, although it was possible to estimate from the burst patterns observed on an oscilloscope that many of the particles were large (>>1.0 μm in diameter). Although particle size is usually important to laser velocimetry accuracy, it was not found to be critical in this instance because only the free-stream velocity was measured without a model in the test section and velocity gradients were small. The typical rate of occurrence and concentration of the measured particles were on the order of 10 to 20 per second and 10^6 per cubic meter, respectively.

CONCLUSION

Free-stream velocity measurements have been made in the Langley 0.3-Meter Transonic Cryogenic Tunnel using a low-power (15 mW) laser velocimeter. These measurements were obtained in an empty test section for the following nominal tunnel conditions: Mach numbers from 0.20 to 0.77, temperatures from 100 to 250 K, and pressures 1.0 to 1.5 atm. The laser velocimeter measurements typically agreed to within 1 percent with velocities calculated from tunnel parameters. The overall normalized standard deviation ($\sigma_m/\bar{V}_m$) was less than 1 percent. Vibrations and the inherent tunnel contraction due to temperature changes had negligible effect on the optical alignment and the laser operation. These favorable results recommend that laser velocimeter be further investigated for future use in this facility.

Langley Research Center
National Aeronautics and Space Administration
Hampton, VA 23665
March 10, 1981

APPENDIX

CORRECTION FOR THE EFFECTS OF SIGNAL PROCESSING BY HIGH-SPEED BURST COUNTER ON TURBULENCE INTENSITY MEASUREMENTS

by

James F. Meyers

The high-speed burst counter measures the time for a fixed number of cycles in the Doppler burst; errors occur in the normalized standard deviation (or turbulence intensity measurement) due to the digitizing of this time by a digital reference clock. This effect is negligible until the flow turbulence intensity approaches 1 percent, since the true velocity probability density function is described by a histogram of only a few velocity increments. The limit of this effect is when the probability density function is described by a histogram containing only two increments, e.g., 625 and 626 reference clock counts.

In order to determine the equation necessary to correct the data for this effect, the error equations must be developed. In general, there are three error sources due to the high-speed burst counter: (1) threshold limit error, (2) clock synchronization error, and (3) quantizing error. The threshold limit error is due to the use of a nonzero volt Schmidt trigger to digitize the Doppler burst. Since the high-pass filtered Doppler burst has a Gaussian envelope, a constant voltage trigger trips at different phases for adjacent cycles in the Doppler burst. Present state-of-the-art high-speed burst counters use a true-zero-crossing detector which eliminates this error if the Doppler signal is properly filtered. Since this was the case in the present test, this error source is not discussed further. The clock synchronization error is due to the mismatch of the randomly occurring Doppler burst with the start of a clock cycle. The result of this error is a 1-clock-count uncertainty in the measurement for Doppler bursts containing signals of the same frequency. The quantizing error is due to the digitizing of time during which a fixed number of Doppler cycles occur. Since the time to be measured is a continuous analog function, the quantizing error has an uncertainty of ±1 clock count.

Once the aforementioned error sources have been described, they may be combined for a total error in the mean velocity measurement and a total error in the turbulence intensity measurement. From these equations, the error correction equations may be developed and used to correct the measurements made with the laser velocimeter.

Basic Statistical Equations

The two quantities in the error analysis described herein are the mean and the standard deviation of the measured velocity ensemble. The standard deviation measurement is then used to solve for the turbulence intensity γ (equal to $\sigma/\bar{V}$) of the flow. The expected value of the measured velocity (or

mean velocity, $\bar{V}_m$) may be approximated by a Taylor series in terms of the true mean velocity $\bar{V}$:

$$E\{V_m\} = \bar{V}_m = f(\xi) + (x - \xi)f'(\xi) + \left(\frac{x - \xi}{2!}\right)^2 f''(\xi) + \ldots . \qquad (A1)$$

where

$$f(\xi) = E\{V_i\} = \bar{V}$$

$$f'(\xi) = E\{V_i^2\} = \bar{V}^2(1 + \gamma^2)$$

$$f''(\xi) = E\{V_i^3\} = \bar{V}^3(1 + 3\gamma^2)$$

and where the expected value of the random variable η_i is

$$(x - \xi)^2 = E\{\eta_i^2\}$$

Note that since η_i and V_i are independent,

$$(x - \xi)f'(\xi) = E\{\eta_i V_i^2\} = E\{\eta_i\}\ E\{V_i^2\}$$

Thus,

$$\bar{V}_m = \bar{V} + \bar{V}^2(1 + \gamma^2)\ E\{\eta_i\} + \frac{\bar{V}^3(1 + 3\gamma^2)}{2} E\{\eta_i^2\} \qquad (A2)$$

The definition of variance (σ_m^2) is

$$\sigma_m^2 = E\{V_m^2\} - \bar{V}_m^2$$

where

$$E\{V_m^2\} = E\{(V_i + \eta_i V_i^2 + \eta_i^2 V_i^3)^2\} \qquad (A3)$$

and since η_i and V_i are independent,

APPENDIX

$$E\{V_m^2\} = E\{V_i^2\} + 2\,E\{n_i\}\,E\{V_i^3\} + 3\,E\{n_i^2\}\,E\{V_i^4\}$$

$$+ 2\,E\{n_i^3\}\,E\{V_i^5\} + E\{n_i^4\}\,E\{V_i^6\} \qquad \text{(A4)}$$

The moments of V_i are

$$E\{V_i^2\} = \bar{V}^2(1 + \gamma^2)$$

$$E\{V_i^3\} = \bar{V}^3(1 + 3\gamma^2)$$

$$E\{V_i^4\} = \bar{V}^4(1 + 6\gamma^2 + 3\gamma^4)$$

$$E\{V_i^5\} = \bar{V}^5(1 + 10\gamma^2 + 15\gamma^4)$$

$$E\{V_i^6\} = \bar{V}^6(1 + 15\gamma^2 + 45\gamma^4 + 5\gamma^6)$$

T' is,

$$E\{V_m^2\} = \bar{V}^2(1 + \gamma^2) + 2\bar{V}^3(1 + 3\gamma^2)\,E\{n_i\} + 3\bar{V}^4(1 + 6\gamma^2 + 3\gamma^4)\,E\{n_i^2\}$$
$$+ 2\bar{V}^5(1 + 10\gamma^2 + 15\gamma^4)\,E\{n_i^3\} + \bar{V}^6(1 + 15\gamma^2 + 45\gamma^4 + 5\gamma^6)\,E\{n_i^4\} \qquad \text{(A5)}$$

and from equation (A2),

$$\bar{V}_m^2 = \bar{V}^2 + 2\bar{V}^3(1 + \gamma^2)\,E\{n_i\} + 2\bar{V}^4(1 + 3\gamma^2)\,E\{n_i^2\} + \bar{V}^4(1 + \gamma^2)^2\,E^2\{n_i\}$$
$$+ 2\bar{V}^5(1 + \gamma^2)(1 + 3\gamma^2)\,E\{n_i\}\,E\{n_i^2\} + \bar{V}^6(1 + 3\gamma^2)^2\,E^2\{n_i^2\} \qquad \text{(A6)}$$

Then,

$$\sigma_m^2 = \sigma^2 + 4\bar{V}^3\gamma^2\,E\{n_i\} + \bar{V}^4(1 + 12\gamma^2 + 9\gamma^4)\,E\{n_i^2\} - \bar{V}^4(1 + \gamma^2)^2\,E^2\{n_i\}$$
$$+ 2\bar{V}^5(1 + 10\gamma^2 + 15\gamma^4)\,E\{n_i^3\} - 2\bar{V}^5(1 + \gamma^2)(1 + 3\gamma^2)\,E\{n_i\}\,E\{n_i^2\}$$
$$+ \bar{V}^6(1 + 15\gamma^2 + 45\gamma^4 + 5\gamma^6)\,E\{n_i^4\} - \bar{V}^6(1 + 3\gamma^2)^2\,E^2\{n_i^2\} \qquad \text{(A7)}$$

APPENDIX

Clock Synchronization

The uncertainty in the clock synchronization is a uniform random variable within the band from 0 to -1 clock pulse. Thus the functions of η_i become

$$E\{\eta_i\} = \frac{1}{2}\left(\frac{1}{MS_f f_c}\right) = \frac{1}{2\bar{V}}\left(\frac{f_D}{Mf_c}\right) = \frac{q}{2\bar{V}}$$

$$E\{\eta_i^2\} = \frac{1}{3}\left(\frac{1}{MS_f f_c}\right)^2 = \frac{1}{3\bar{V}^2}\left(\frac{f_D}{Mf_c}\right)^2 = \frac{q^2}{3\bar{V}^2}$$

$$E\{\eta_i^3\} = \frac{1}{4}\left(\frac{1}{MS_f f_c}\right)^3 = \frac{1}{4\bar{V}^3}\left(\frac{f_D}{Mf_c}\right)^3 = \frac{q^3}{4\bar{V}^3}$$

$$E\{\eta_i^4\} = \frac{1}{5}\left(\frac{1}{MS_f f_c}\right)^4 = \frac{1}{5\bar{V}^4}\left(\frac{f_D}{Mf_c}\right)^4 = \frac{q^4}{5\bar{V}^4}$$

where

M number of Doppler cycles used

S_f fringe spacing

f_c reference clock frequency

f_D Doppler frequency $= \dfrac{\bar{V}}{S_f}$

$q = \dfrac{f_D}{Mf_c}$

In the case under study, the number of Doppler cycles used is eight, the reference clock frequency is 500 MHz, and the maximum Doppler frequency possible is 100 MHz. The maximum value of q is 0.025 which is much greater than q^2; thus all terms q^n with $n \geq 2$ in equations (A2) and (A7) are neglected. Equations (A2) and (A7) now become

APPENDIX

$$\bar{V}_m = \bar{V} + \bar{V}^2(1 + \gamma^2)\ E\{\eta_i\} = \bar{V}\left[1 + \frac{q}{2}(1 + \gamma^2)\right] \tag{A8}$$

$$\sigma_m^2 = \sigma^2 + 4\bar{V}^3\gamma^2\ E\{\eta_i\} = \sigma^2(1 + 2q) \tag{A9}$$

The error in the mean velocity ε_V is

$$\varepsilon_V = \frac{\bar{V}_m - \bar{V}}{\bar{V}} = \frac{q}{2}(1 + \gamma^2) \tag{A10}$$

and the error in turbulence intensity ε_γ is

$$\varepsilon_\gamma = \frac{\gamma_m - \gamma}{\gamma} \approx \frac{q}{2}(1 - \gamma^2) \tag{A11}$$

Quantizing Error

The uncertainty in the timing of the Doppler signal due to the digitizing of time by the reference clock is a uniform random variable within a band from -1 clock pulse to +1 clock pulse. Thus the functions of η_i become

$$E\{\eta_i\} = 0$$

$$E\{\eta_i^2\} = \frac{1}{3}\left(\frac{1}{MS_f f_c}\right)^2 = \frac{1}{3\bar{V}^2}\left(\frac{f_D}{Mf_c}\right)^2 = \frac{q^2}{3\bar{V}^2}$$

$$E\{\eta_i^3\} = 0$$

$$E\{\eta_i^4\} = \frac{1}{5}\left(\frac{1}{MS_f f_c}\right)^4 = \frac{1}{5\bar{V}^4}\left(\frac{f_D}{Mf_c}\right)^4 = \frac{q^4}{5\bar{V}^4} \approx 0$$

Then equations (A2) and (A7) become (q^4 terms neglected)

APPENDIX

$$\bar{V}_m = \bar{V} + \bar{V}^3(1 + 3\gamma^2)\left(\frac{q^2}{3\bar{V}^2}\right) = \bar{V}\left[1 + \frac{q^2}{3}(1 + 3\gamma^2)\right] \tag{A12}$$

$$\sigma_m^2 = \sigma^2 + \bar{V}^4(1 + 12\gamma^2 + 9\gamma^4)\left(\frac{q^2}{3\bar{V}^2}\right) = \sigma^2 + \frac{\bar{V}^2q^2}{3}(1 + 12\gamma^2 + 9\gamma^4) \tag{A13}$$

The error in the mean velocity ε_V is

$$\varepsilon_V = \frac{\bar{V}_m - \bar{V}}{\bar{V}} = \frac{q^2}{3}(1 + 3\gamma^2) \tag{A14}$$

and the error in turbulence intensity ε_γ is

$$\varepsilon_\gamma = \frac{\gamma_m - \gamma}{\gamma} \approx \frac{q^2}{6\gamma^2} \tag{A15}$$

Data Correction

To correct the data on the basis of the equations derived for the aforementioned high-speed burst counter errors, the nature of the errors must be determined and their significance understood. The error in the mean velocity measurement due to clock synchronization is biased toward a higher velocity than the true velocity since the measurements are always correct for 1 clock count less. The error in the mean velocity measurement due to quantizing error is a random error since the probability that there will be one too many clock pulses is equal to the probability that there will be one too few. Both errors in the turbulence intensity measurement are positive bias errors.

The total mean velocity error is determined by combining equations (A10) and (A14)

$$\varepsilon_V = \frac{q}{2}(1 + \gamma^2) \pm \frac{q^2}{3}(1 + 3\gamma^2) \tag{A16}$$

However, as stated above, q is much greater than q^2; thus the second term is neglected and only a bias error described by equation (A10) is considered. Based on equation (A10), the true mean velocity may be found from

$$\bar{V} = \frac{2\bar{V}_m}{2 + q(1 + \gamma^2)} \tag{A17}$$

The turbulence intensity error is determined by combining equations (A11) and (A15):

$$\epsilon_\gamma = \frac{q}{2}(1 - \gamma^2) + \frac{q^2}{6\gamma^2} \tag{A18}$$

At large values of turbulence intensity, the first term is dominant even though its magnitude is very small. However as the turbulence intensity decreases, the second term becomes dominant and its magnitude becomes significant. Thus the error correction is developed from the second term, which is the quantizing error given in equation (A15), and used to correct the data at low turbulence intensities. The resulting expression is then simplified using binomial series expansion techniques which yield the following expression:

$$\gamma \approx \left(\gamma_m^2 - \frac{q^2}{3}\right)^{1/2} \tag{A19}$$

In order to verify equation (A19), an extremely stable FM generator was used as a single source for a high-speed burst counter and a frequency tracker. The output from the frequency tracker was used as the standard for determining the input turbulence intensity. The measurement errors for the high-speed burst counter as a function of input turbulence intensity are shown by the symbols in figure 15. The curve is the expected error based on the calculations from equation (A15). Figure 16 contains the results from comparing the measured turbulence intensity from the high-speed burst counter with the input turbulence intensity (circular symbols). If the measured data are correct, they lie along the 45° line. As shown in the figure, the quantizing error becomes significant at a turbulence intensity of 1 percent. When the turbulence intensity decreases to the point where all the data are contained within two reference clock counts (the horizontal line at 0.36 percent for this test case), the data and any correction of the data are unreliable. By applying equation (A19), the data are corrected and are shown by the triangular symbols.

Thus the errors in the velocity measurements due to the high-speed burst counter may be removed since both the error in the mean velocity measurement and the error in the turbulence intensity measurement are bias errors and may be removed using equations (A17) and (A19).

REFERENCES

1. Hoad, Danny R.; Meyers, James F.; Young, Warren H., Jr.; and Hepner, Timothy E.: Correlation of Laser Velocimeter Measurements Over a Wing With Results of Two Prediction Techniques. NASA TP-1168, 1978.

2. Young, Warren H., Jr.; Meyers, James F.; and Hepner, Timothy E.: Laser Velocimeter Systems Analysis Applied to a Flow Survey Above a Stalled Wing. NASA TN D-8408, 1977.

3. Gartrell, Luther R.; and Rhodes, David B.: A Scanning Laser-Velocimeter Technique for Measuring Two-Dimensional Wake-Vortex Velocity Distributions. NASA TP-1661, 1980.

4. Gartrell, Luther R.; and Jordan, Frank L., Jr.: Demonstration of Rapid-Scan Two-Dimensional Laser Velocimetry in the Langley Vortex Research Facility for Research in Aerial Applications. NASA TM-74081, 1977.

5. Orloff, Kenneth L.; and Grant, George R.: The Application of Laser Doppler Velocimetry to Trailing Vortex Definition and Alleviation. NASA TM X-62243, 1973.

6. Ray, Edward J.; Ladson, Charles L.; Adcock, Jerry B.; Lawing, Pierce L.; and Hall, Robert M.: Review of Design and Operational Characteristics of the 0.3-Meter Transonic Cryogenic Tunnel. NASA TM-80123, 1979.

TABLE I.- LASER VELOCIMETER DATA FOR NOMINAL TEST CONDITIONS

File number	Nominal tunnel calibration		N	$\bar{V}_m$, m/s	$\Delta\bar{V}_m$, m/s	σ_m, m/s	$\Delta\sigma_m$, m/s	$\bar{V}_c$, m/s	$\frac{\bar{V}_m - \bar{V}_c}{\bar{V}_c}$, percent	$\frac{\sigma_m}{\bar{V}_m}$, percent
	M_∞	T_t, K								
12	0.30	100	1023	63.7	0.01	0.39	0.01	62.3	2.25	0.6
13	.30	100	1022	63.8	.01	.38	.01	63.0	1.27	.6
14	.40	100	993	76.7	.02	.47	.01	76.2	.66	.6
15	.40	100	992	76.6	.01	.42	.01	76.3	.39	.5
16	.50	100	1024	94.6	.02	.52	.01	94.1	.53	.5
17	.50	100	1024	94.6	.02	.44	.01	94.0	.64	.5
18	.50	100	1023	94.6	.02	.48	.01	94.2	.43	.5
19	.50	100	1019	94.6	.02	.56	.01	94.7	-.11	.6
20	.60	100	1018	112.1	.03	.88	.01	111.9	.18	.8
21	.60	100	1017	112.3	.03	.93	.01	112.1	.18	.8
22	.60	100	1016	112.3	.03	.90	.01	112.3	0	.8
23	.70	100	1024	129.7	.03	.70	.02	129.1	.46	.5
24	.70	100	1024	129.6	.03	.70	.02	129.5	.08	.5
25	.70	100	1023	129.8	.02	.68	.02	129.3	.39	.5
26	.77	100	1009	139.4	.04	1.17	.03	139.6	-.14	.8
27	.77	100	1022	140.7	.03	.98	.02	140.8	-.07	.7
28	.77	100	1018	140.3	.03	1.01	.02	140.1	.14	.7
29	.77	100	1021	140.6	.03	.95	.02	140.3	.21	.7
31	.50	100	1023	94.6	.02	.56	.01	94.1	.53	.6
32	.30	100	1023	57.6	.01	.42	.01	57.2	.70	.7
33	.30	100	1023	57.7	.01	.43	.01	56.8	1.58	.7
34	.30	100	1023	57.5	.01	.39	.01	57.0	.88	.7

TABLE I.- Concluded

File number	Nominal tunnel calibration		N	$\bar{V}_m$, m/s	$\Delta\bar{V}_m$, m/s	σ_m, m/s	$\Delta\sigma_m$, m/s	$\bar{V}_c$, m/s	$\frac{\bar{V}_m - \bar{V}_c}{\bar{V}_c}$, percent	$\frac{\sigma_m}{\bar{V}_m}$, percent
	M_∞	T_t, K								
37	0.20	150	919	51.0	0.02	0.52	0.02	49.4	3.24	1.0
38	.30	150	992	74.6	.02	.63	.01	73.8	1.08	.8
39	.40	150	1012	99.1	.03	1.07	.05	99.2	-.10	1.1
40	.50	150	1020	120.6	.04	1.17	.03	120.8	-.17	1.0
42	.50	150	1021	121.5	.04	1.09	.03	120.9	.50	.4
43	.70	150	1023	167.0	.04	1.11	.03	165.8	.72	.7
44	.70	150	1023	167.2	.04	1.18	.03	166.3	.54	.7
45	.77	150	1017	181.4	.05	1.52	.04	179.7	.95	.8
46	.77	150	1017	181.5	.05	1.41	.04	180.4	.61	.8
48	.40	200	1021	113.3	.03	.93	.03	113.1	.18	.8
49	.50	200	1012	142.2	.03	.98	.02	141.6	.42	.7
50	.60	200	1021	168.1	.04	1.18	.03	166.6	.90	.7
51	.60	200	1018	168.2	.04	1.13	.03	167.0	.72	.7
52	.70	200	999	193.5	.04	.99	.03	192.5	.52	.5
53	.70	200	997	193.5	.04	.96	.03	191.8	.89	.5
54	.77	200	1022	209.9	.06	1.75	.04	209.8	.05	.8
55	.77	200	1022	209.4	.06	1.72	.04	209.2	.10	.8
56	.60	200	1023	167.7	.04	1.16	.04	166.2	.90	.7
57	.60	250	1020	188.3	.04	1.16	.04	187.3	.53	.6
58	.70	250	649	215.8	.08	1.88	.06	215.0	.37	.8
59	.77	250	936	235.2	.07	1.68	.06	234.5	.30	.7

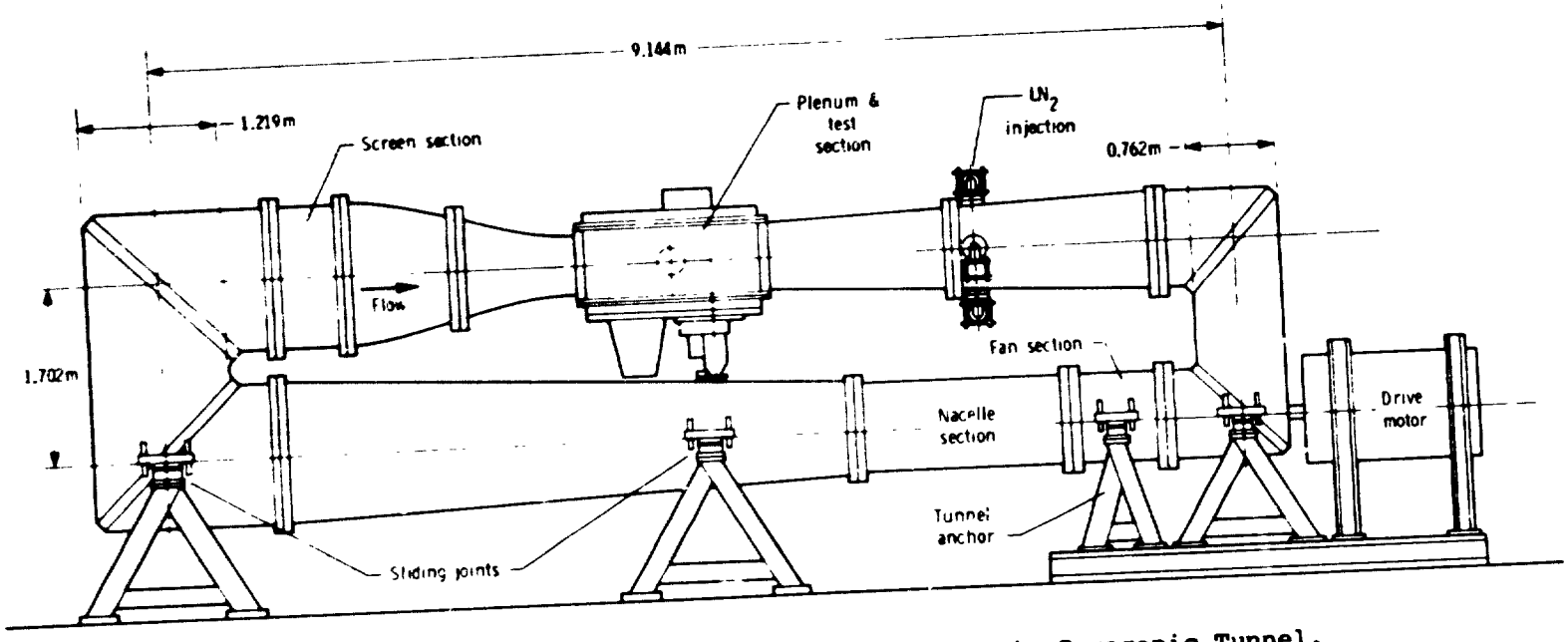

Figure 1.- Schematic of Langley 0.3-Meter Transonic Cryogenic Tunnel.

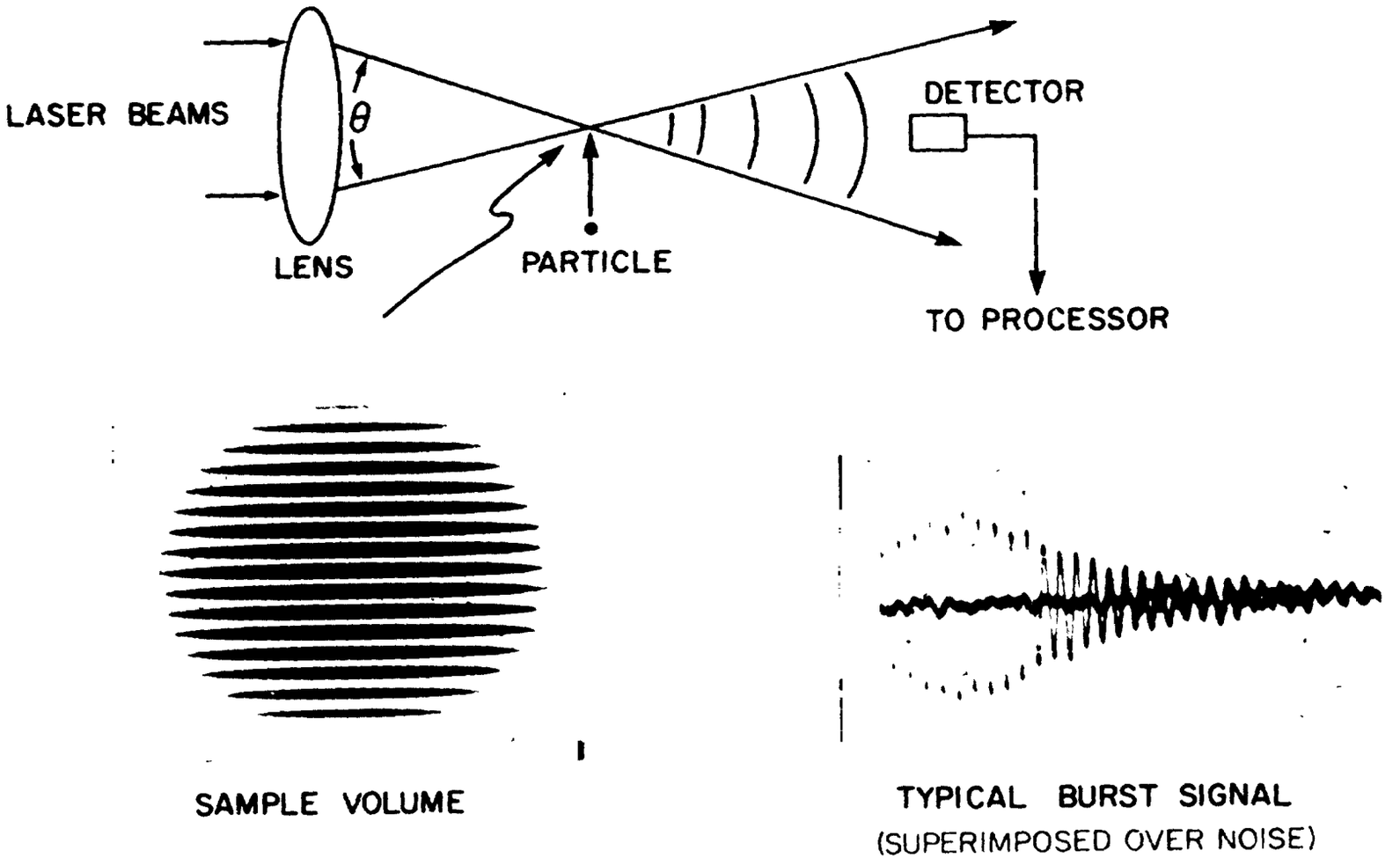

Figure 2.- Laser velocimeter technique.

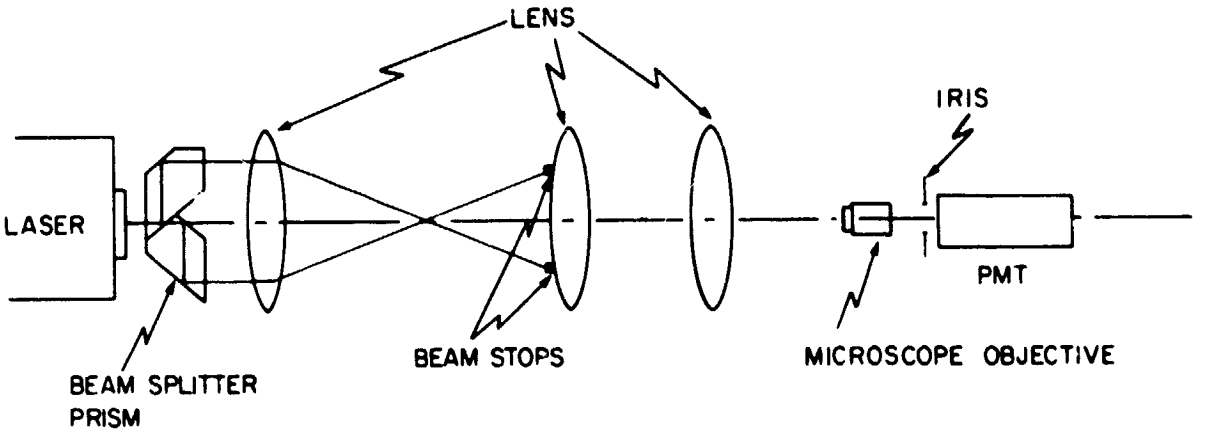

Figure 3.- Diagram of the laser velocimeter system.

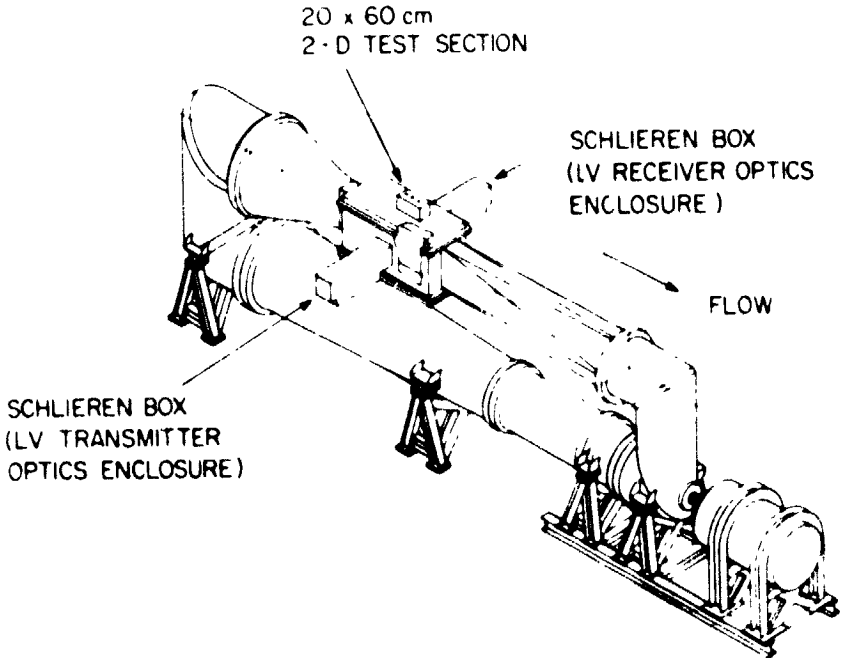

Figure 4.- Metal enclosure for optical system mounted on tunnel test section.

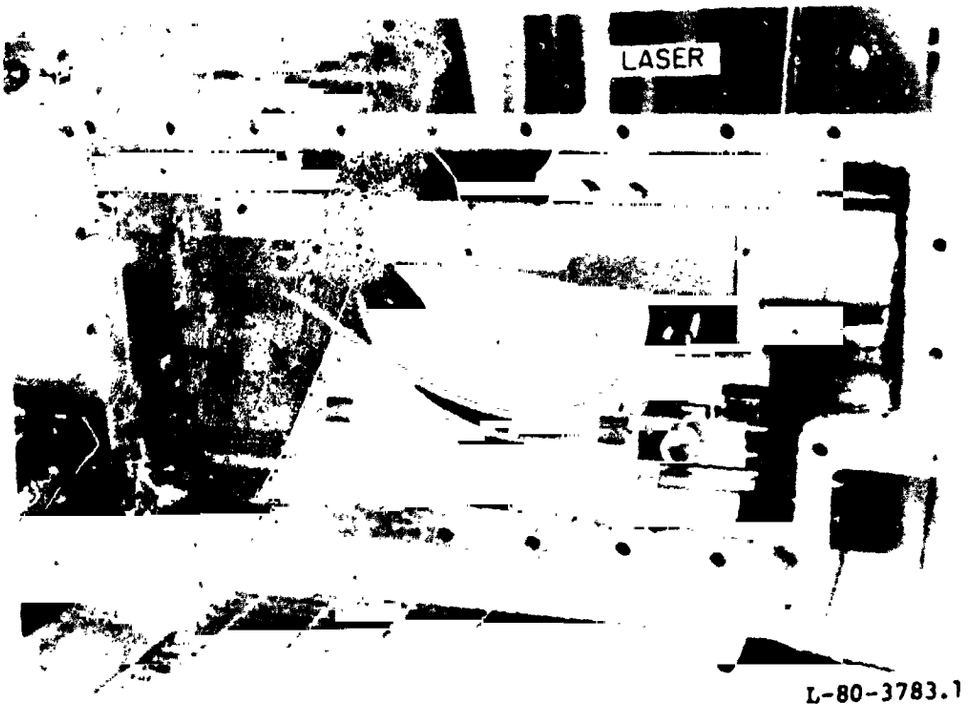

(a) Transmitter section.

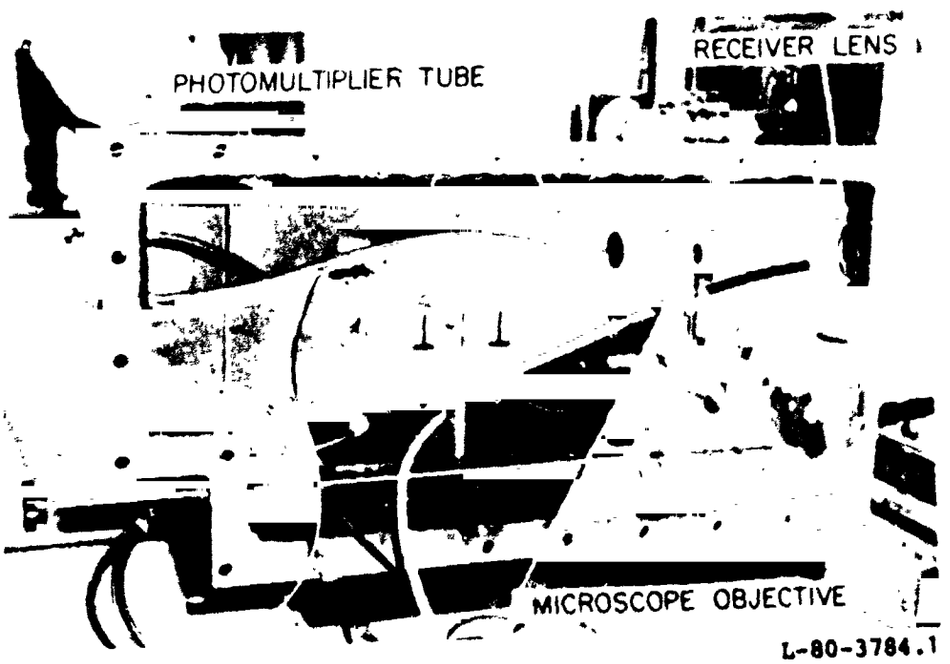

(b) Receiver section.

Figure 5.- Laser velocimeter mounted in metal enclosure.

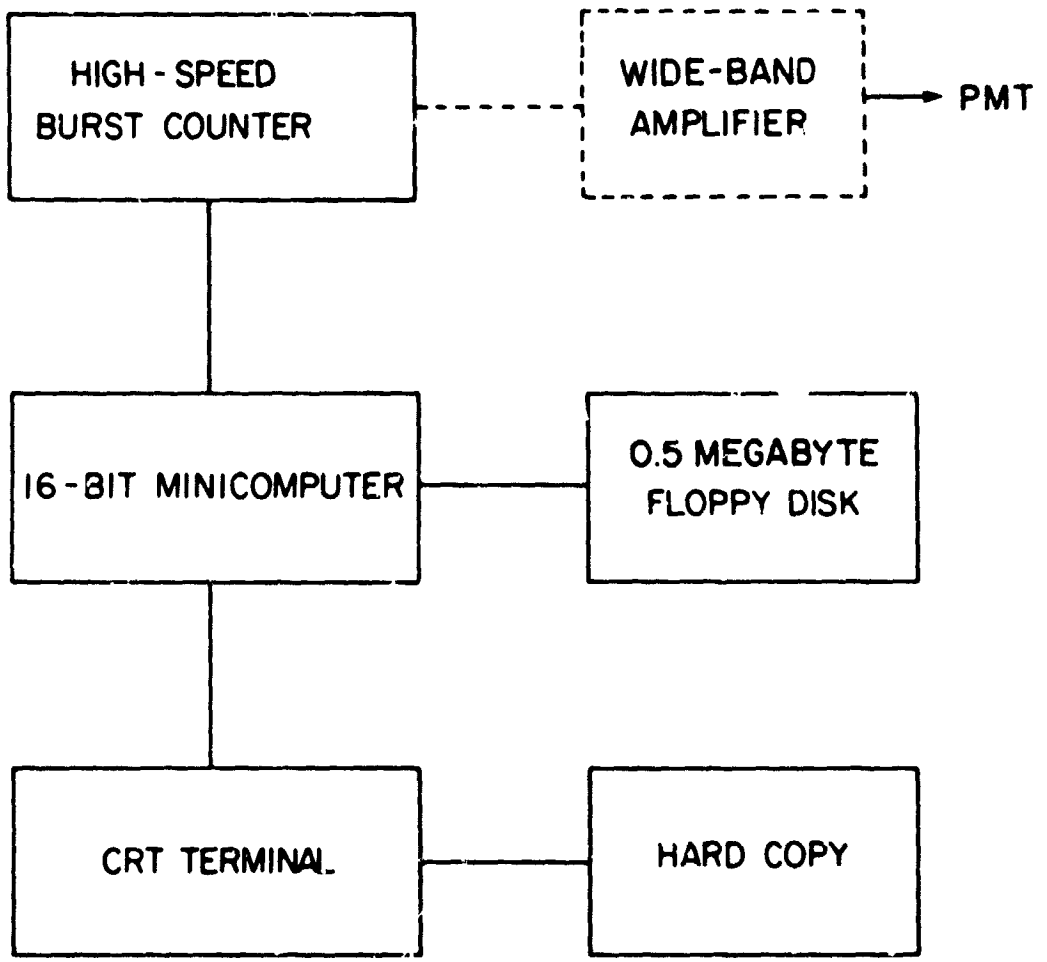

Figure 6.- Block diagram of data acquisition and processing system.

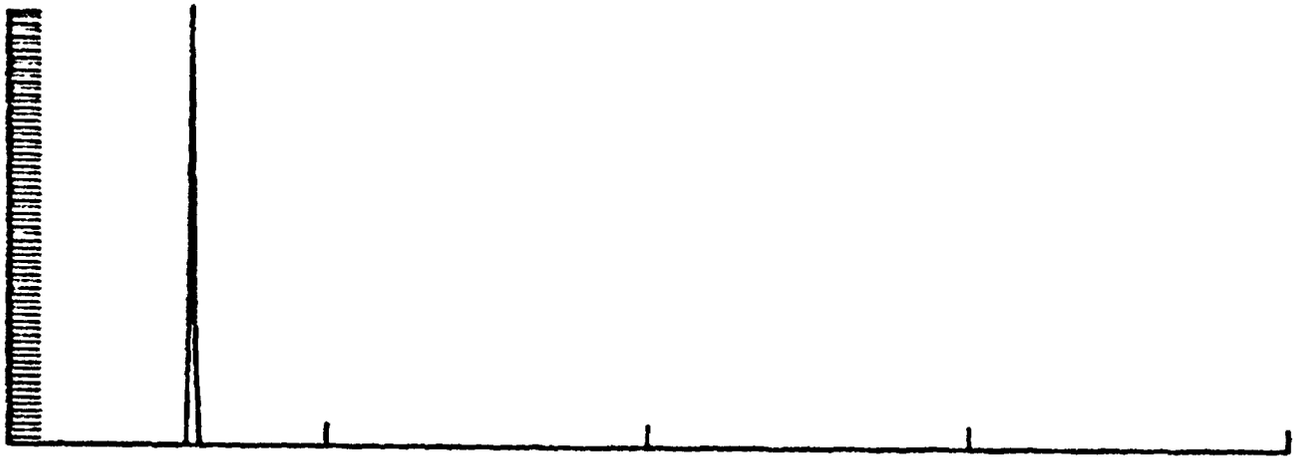

FILE NUMBER - 33

NU OF DATA POINTS = 1023.

MEAN VELOCITY = 57.7382
? MEAN = .0136
SIGMA = .4344
? SIGMA = .0134
SKEW = .4531
EXCESS = 1.9132

Figure 7.- Typical CRT histogram and data display.

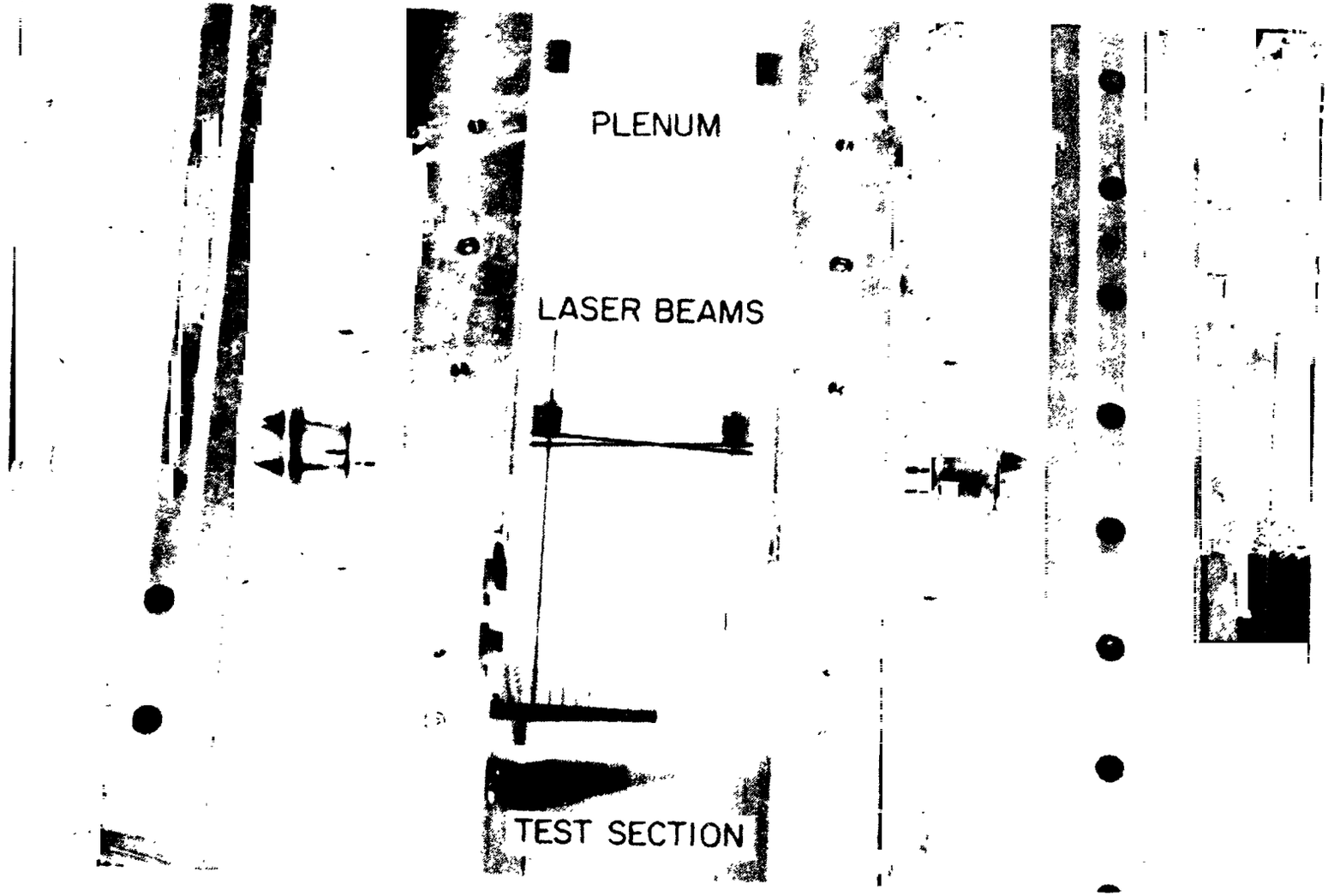

Figure 8.- Laser beams in tunnel test section (top view).

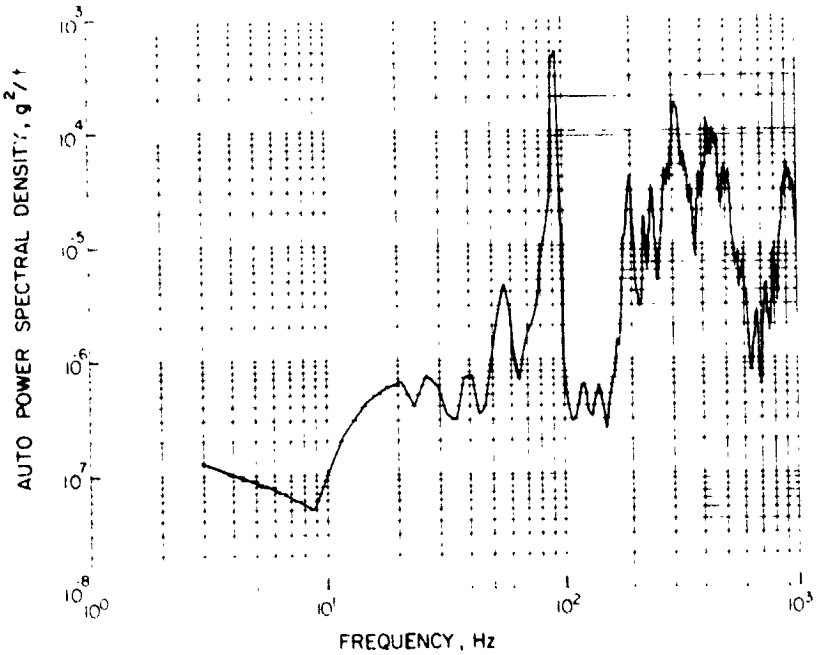

(a) Transmitter enclosure.

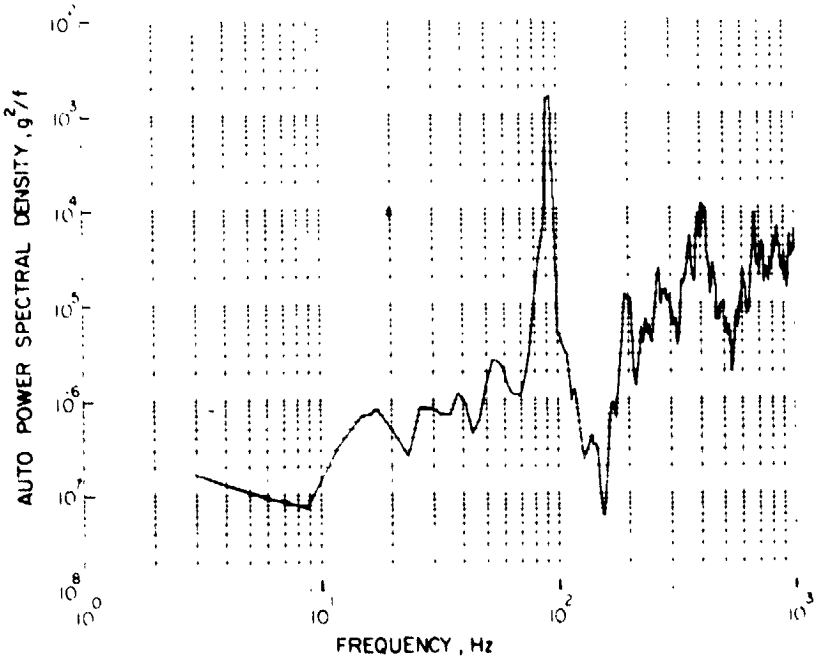

(b) Receiver enclosure.

Figure 9.- Acceleration power spectral density for induced vertical-mode vibrations of LV optics enclosures. $M_\infty = 0.77$; $T_t = 250$ K.

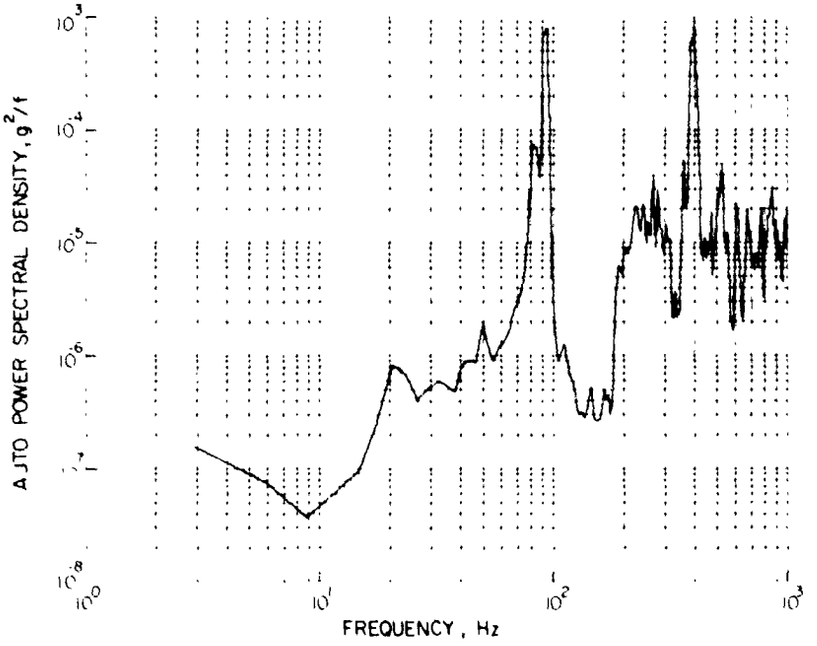

(a) Transmitter enclosure.

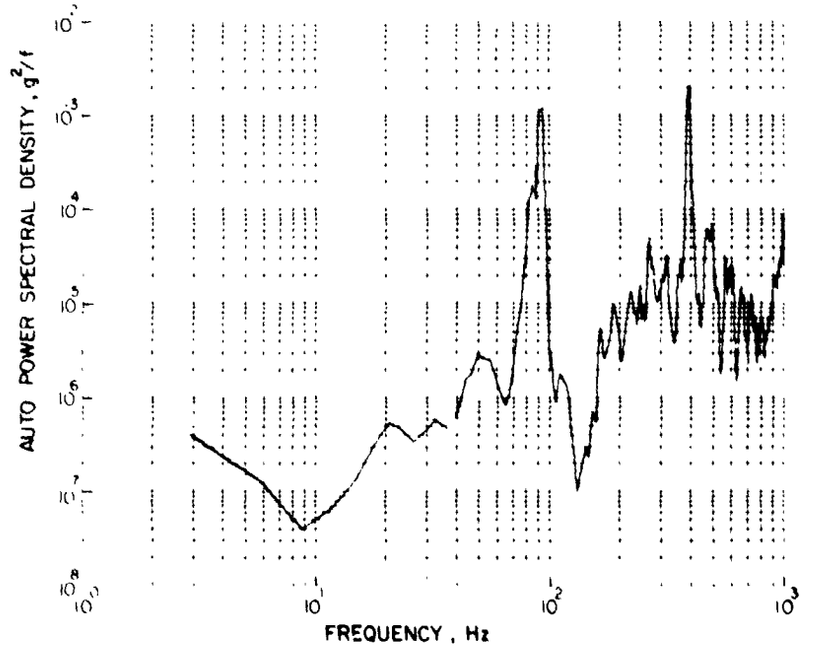

(b) Receiver enclosure.

Figure 10.- Acceleration power spectral density for induced longitudinal-mode vibrations of LV optics enclosures. $M_\infty = 0.77$; $T_\infty = 250$ K.

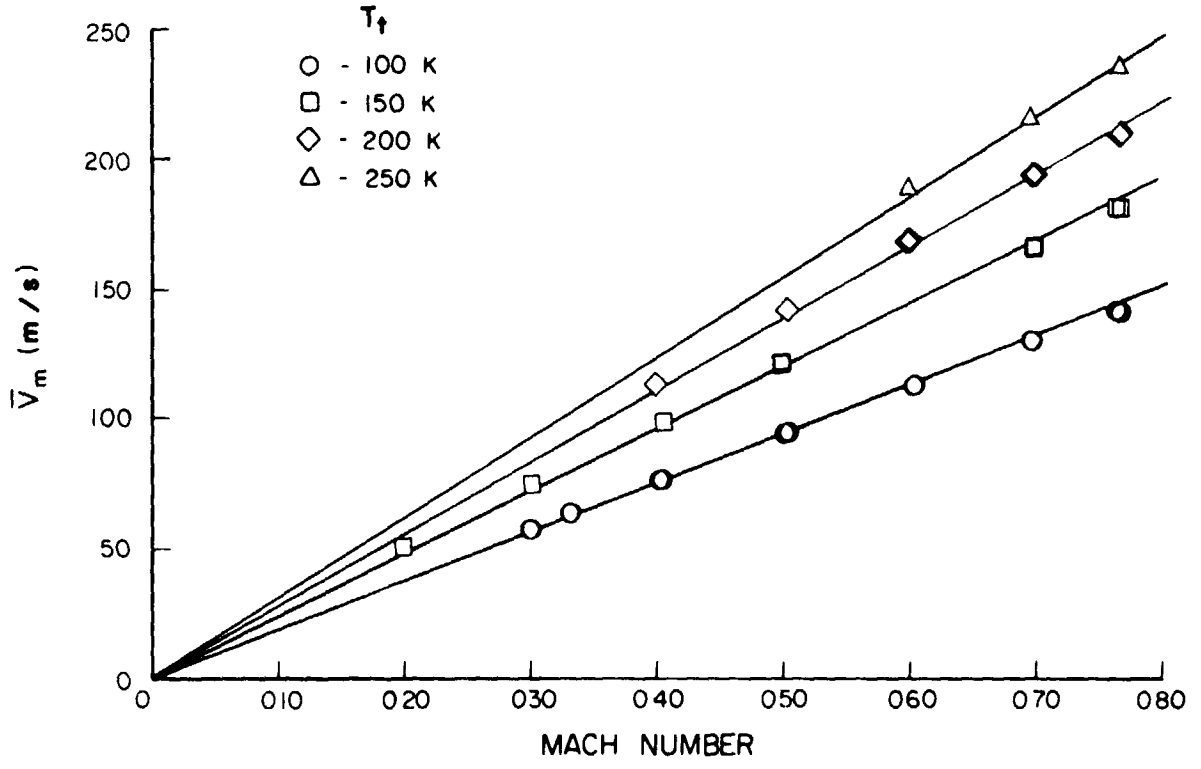

Figure 12.- Measured mean velocity as a function of total temperature and Mach number.

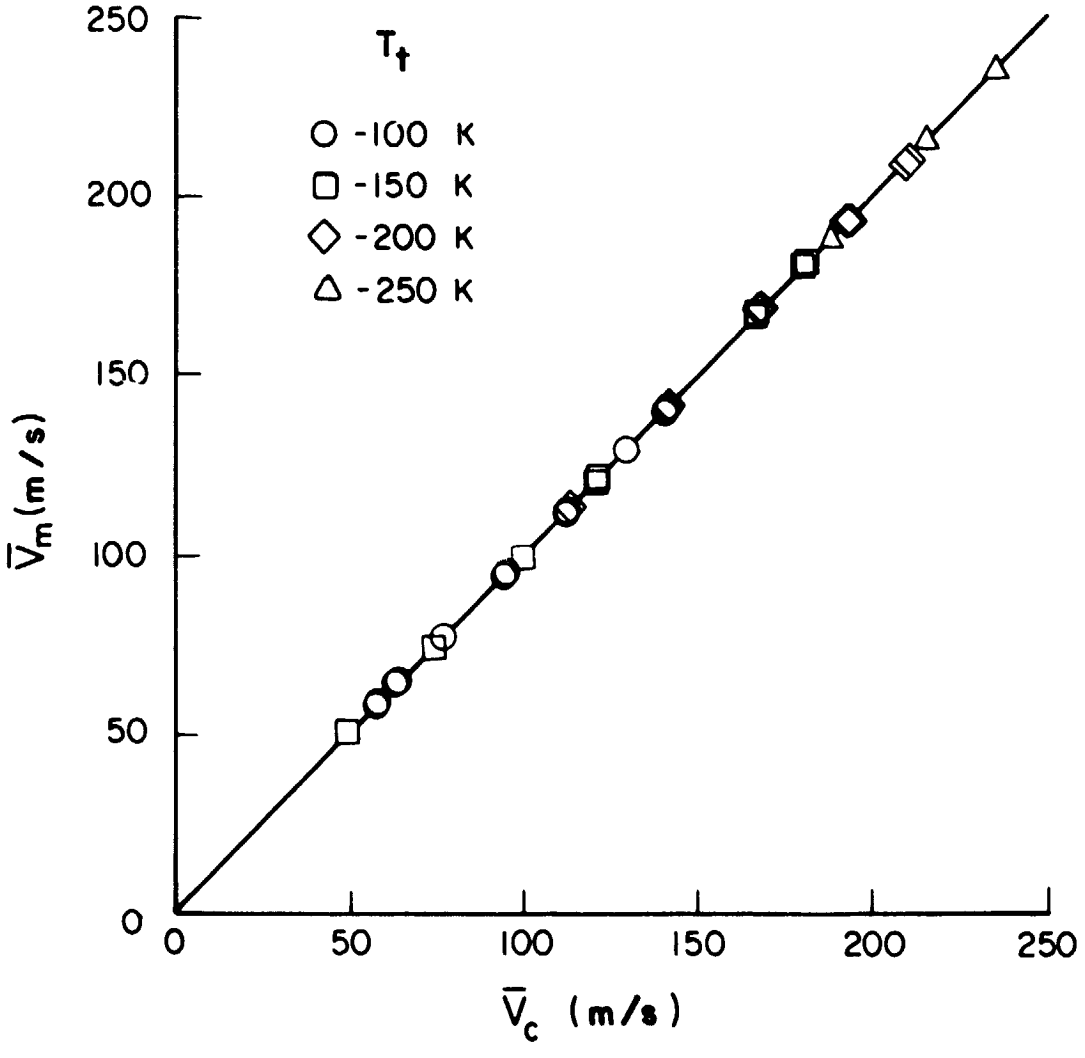

Figure 13.- Measured mean velocity versus calculated mean velocity.

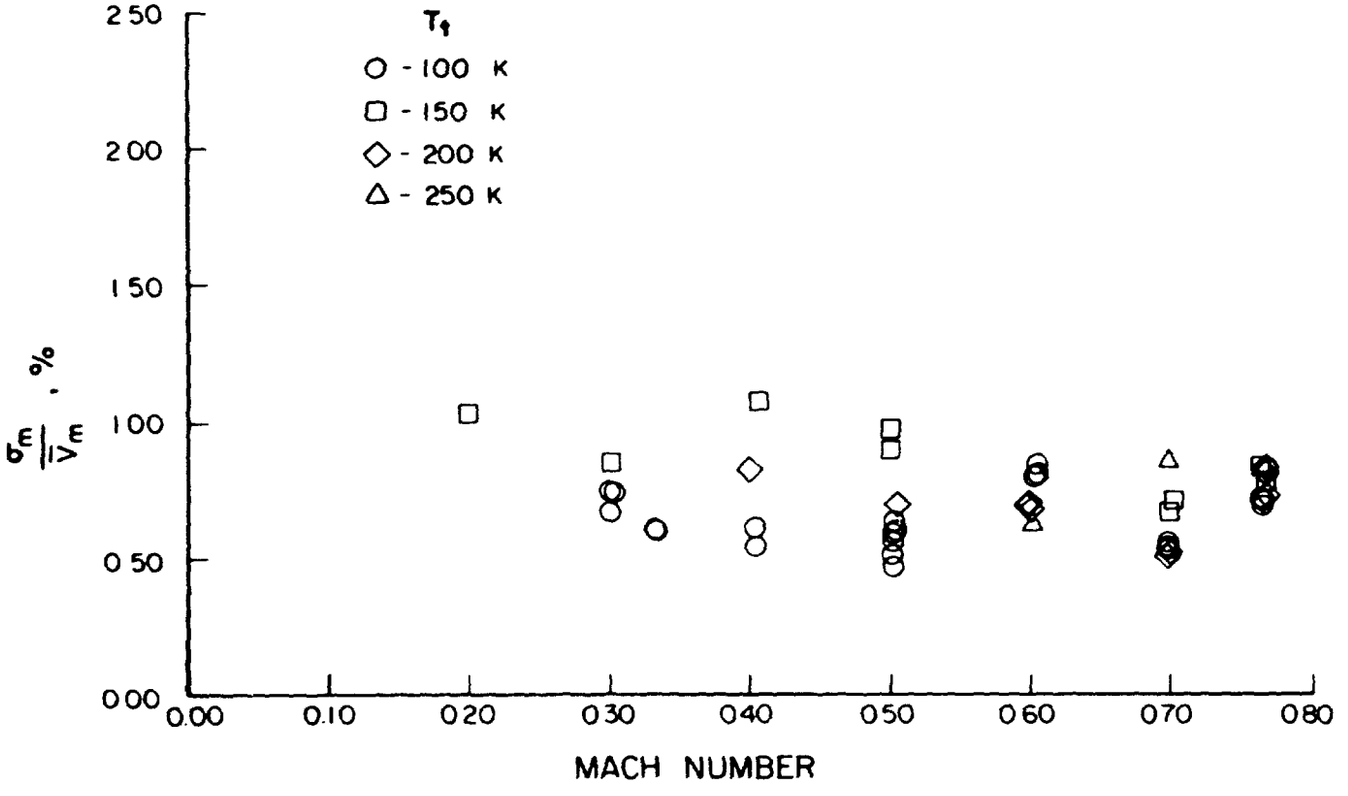

Figure 14.- Normalized standard deviation as a function of total temperature and Mach number.

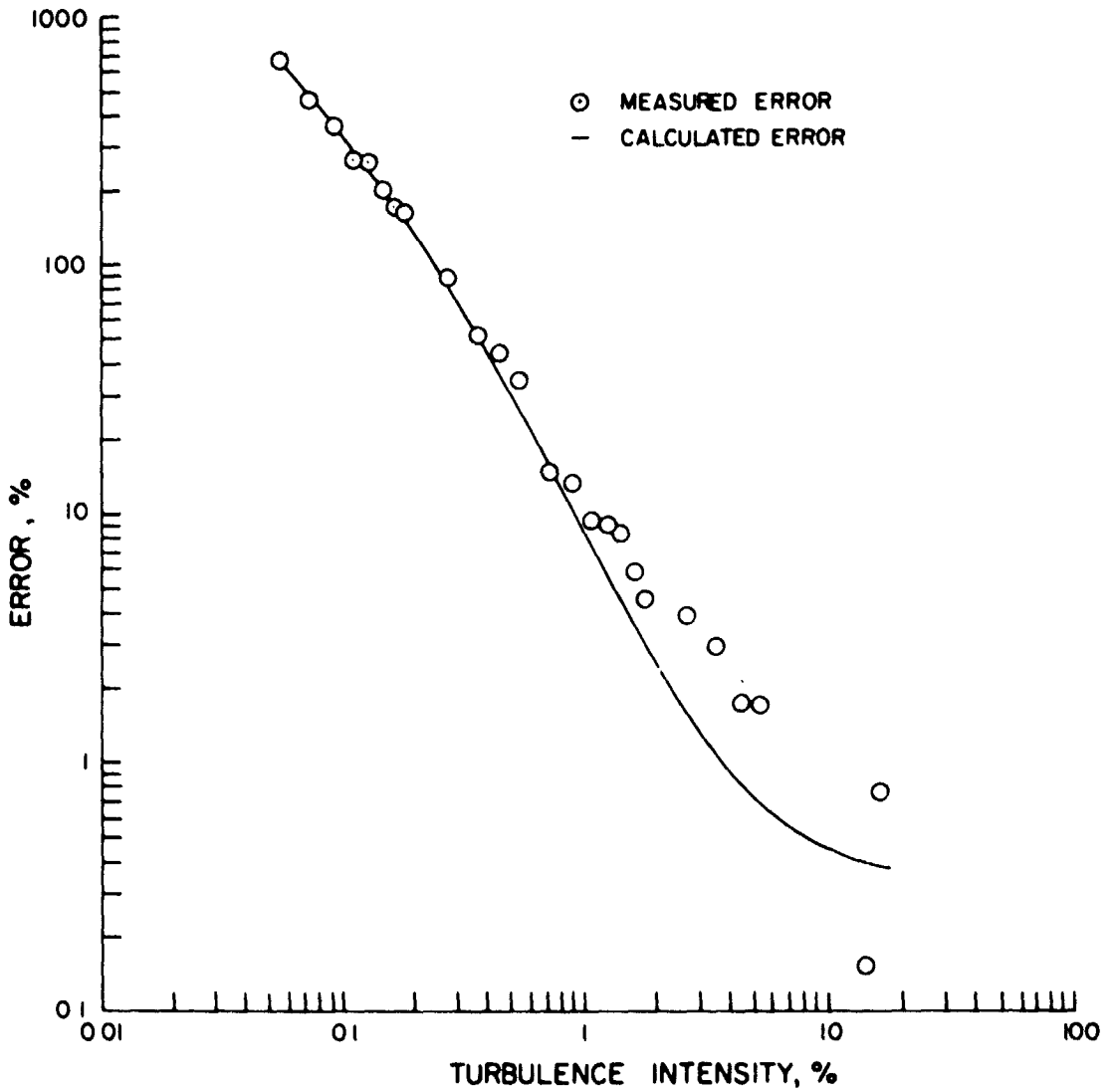

Figure 15.- Turbulence intensity error in high-speed burst counter measurement.

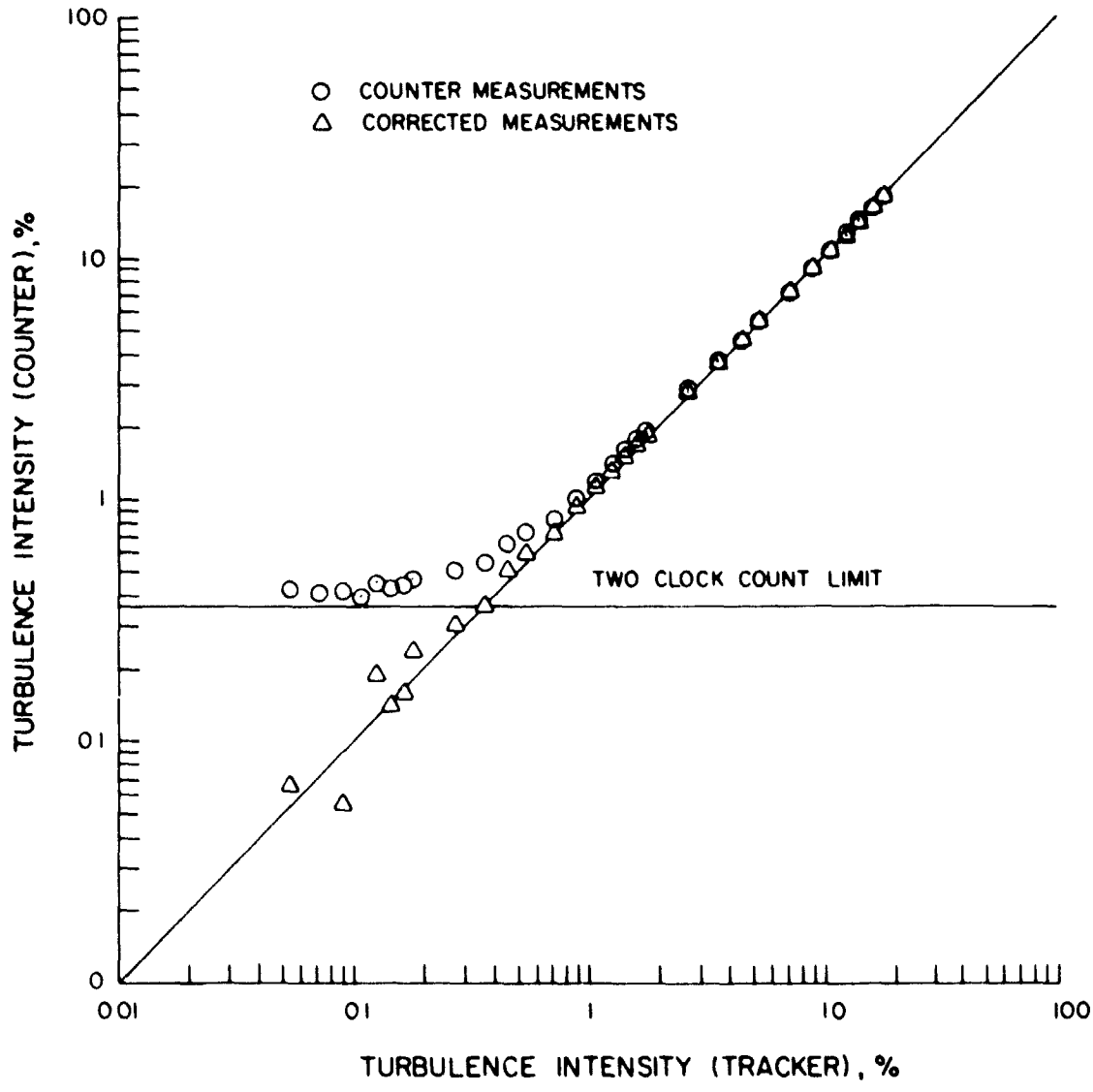

Figure 16.- Turbulence intensity measurements by a high-speed burst counter and corrected data.